P/S separation of OBS data by inversion in a homogeneous medium

Ohad Barak

ABSTRACT

A separation of pressure waves from shear waves in OBS data prior to processing can improve the resulting image. I present a nearly medium-independent P/S separation method, which operates by reconstructing the observed data using a homogeneous medium. The closer the homogeneous medium parameters are to the actual parameters of the medium in which the receivers are planted, the better the separation results. Synthetic tests indicate that the proposed method works reliably for land data even when using wrong medium parameters, but cannot work for OBS data in its current configuration.

INTRODUCTION

Ocean-bottom seismic (OBS) surveys record four-component data: hydrophone pressure data, vertical particle velocity (or acceleration), and two perpendicular horizontal particle velocities. The receivers are located on the sea bed. The source is typically an airgun fired from near the sea surface.

One problem of OBS and of marine streamer acquisition is the inevitable recording of water surface multiples. These multiples are waves which have reflected off the subsurface, and then bounce off the water surface. Though such waves contain subsurface data, attempting to remove them has been part of the traditional processing flow. Unlike marine streamer data, where the receivers record only pressure waves, in OBS acquisition additional energy is recorded. Since the geophones are coupled to the sea bed, they pick up shear waves and other surface waves as well as compressional waves.

A current implementation for processing of OBS data is to regard the hydrophone component and the vertical particle velocity component as containing P-waves only. PZ summation is applied to these components. It is a weighted summation of the hydrophone and the vertical geophone components, designed to determine the vertical propagation direction of the recorded arrivals (Barr and Sanders, 1989). The basic principle of PZ summation is that the hydrophone and the vertical geophone data will have opposite polarity if the energy they recorded was propagating downward. If that energy was propagating upward, they will have the same polarity. This upgoing/downgoing wavefield direction determination method has been used to create

separate images from the primary arrivals and the mirror arrivals (the ones reflecting off the sea-surface) at the nodes on the sea bottom (Dash et al., 2009). This method is known as "mirror imaging". Separating the imaging process removes artifacts resulting from cross-talk between the upgoing and downgoing wavefields. Additionally, mirror imaging increases the effective aperture of the survey, and provides more information than the upgoing image alone.

Shear waves do not propagate in the water column. Therefore the result of applying PZ summation will be to introduce any non-P energy recorded by the vertical geophone into the summation result. These data will be construed as a P-wave energy recording. When these data are then migrated using acoustic wavefield propagation, they may generate artifacts in the resulting image. A simple graphical demonstration of how PZ-summation can introduce shear wave noise into the summation result can be seen in Figure 1.

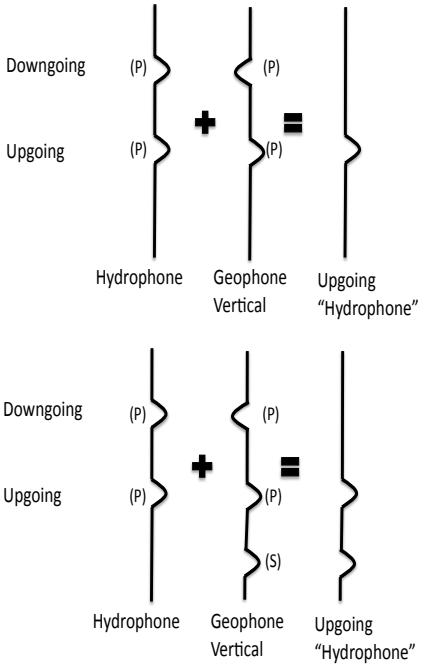

Figure 1: Simplified sketch of PZ summation. Top: For acoustic data, the summation of the hydrophone data and the vertical geophone data will result in the downgoing energy being eliminated, leaving only upgoing pressure data. Bottom: If the data contains shear waves, they will be recorded only by the geophone, and PZ summation will mistakingly add them into a result considered as upgoing pressure data. [**NR**]

A particular problem of OBS data is "Vz noise" (Paffenholz et al., 2006), which may result from surface waves propagating along the water-solid boundary. They can form by shear waves incident on an irregular sea bed topography, or on near surface scatterers. Surface waves can also be generated by upgoing shear-waves incident on a flat sea bed at large angles. Since surface waves appear mainly on the geophone components, they will also contribute to an incorrect PZ summation result if they are not properly removed from the data.

Existing P/S separation methods

Dankbaar (1985); Wapenaar et al. (1990); Amundsen (1993) have shown how to sep-

arate the P and S-waves of OBS data, and also separate between the upgoing and downgoing pressure energy. Their methods require a knowledge of medium parameters in the vicinity of the receivers. Schalkwijk et al. (2003) implement adaptive decomposition, in order to account for the unknown near-surface medium parameters on which the separation depends. This decomposition requires manual identification in each receiver gather of a single time window containing mainly downgoing waves, and of a window that contains mainly upgoing waves. The energy within these windows is then minimized using an itterative process. The filter resulting from this process is inverted for both the local medium parameters and the calibration between the different sensors.

Zhou et al. (2011) propose a novel method of extracting the P-wave data from the geophone components. It involves a complex wavelet transform of the hydrophone and the vertical geophone data. A matching of the geophone data to the predominantly P-wave energy hydrophone data is done in the complex wavelet domain. Afterward, the inverse transform is applied to the result. The end product is a substantially P-only vertical geophone component. PZ summation can then be applied to this component and the recorded hydrophone, to separate the upgoing from the downgoing P-wave.

P/S separation by inversion

If the seismic data were sampled vertically as well as horizontally (i.e. - if receivers were placed at multiple depths as well as on a surface), then the spatial derivatives of the wavefield could be calculated, and the separation between P and S-waves would be trivial. Robertsson and Muyzert (1999) propose doing volumetric recordings of the wavefield using tetrahedral receiver groups, for the purpose of calculating all spatial derivatives and thus separating P from S.

The P/S separation method presented here is a (nearly) medium-independent data-space inversion. The model it attempts to invert for is the wavefield, emitted by a virtual source array at some depth level, which after propagating through a homogeneous medium matches the recorded wavefield at the receiver level.

The basic premise of the separation method is: if there is a good match to the recorded data at the receivers, then there is also a good match to the "true" receiver wavefield at a close proximity to the receivers. The method effectively reconstructs the wavefield at the receiver's vicinity, as it was in the field experiment. Since we now have a volumetric spatial sampling of the wavefield near the receivers, separation operators based on three-dimensional spatial derivatives (i.e. - divergence and curl) are applied to separate P-waves from S-waves.

The synthetic seismic data I use in the following examples are displacement data, which represent geophone acquisition. The elements of the inversion are:

1. Observed data: The original displacement components recorded by the geophones in the field.

2. Model: A virtual source gather, consisting of displacement source functions, injected at some location into a homogeneous elastic medium.

3. Calculated data: The recorded displacements at the receiver level, as a result of the injection of the virtual sources.

4. Desired model: The virtual sources which generate recorded data equal to the observed data.

5. What we actually want: The wavefield displacement values both at the receiver level AND one depth level below them, so that we can apply spatial derivative operators to separate P from S.

THEORY

PZ summation

PZ summation involves summing the pressure data recorded by the hydrophone with the vertical particle velocity data recorded by the geophone, with some scaling factor:

$$\begin{aligned} U(z_r) &= \frac{1}{2}\left[P(z_r) - \beta V_z(z_r)\right], \\ D(z_r) &= \frac{1}{2}\left[P(z_r) + \beta V_z(z_r)\right], \end{aligned} \tag{1}$$

where P is the hydrophone data, V_z is the vertical geophone, U is the upgoing data, D is the downgoing data and z_r is the receiver depth. β is a scaling factor, which is theoretically the acoustic impedance at the wave's incidence angle. In practice, as a result of frequency-dependent instrument response, and as a result of the two different impedances above and below the receivers, β is frequency dependent, propagation-direction dependent, and wave-mode dependent.

Amundsen (1993) does the separation in the $f-k$ domain, and uses $\beta = \frac{\rho\omega}{k_z}$, where $k_z = \sqrt{\frac{\omega^2}{v^2} - k_x^2 - k_y^2}$, and ρ is the density. This implicitly requires a laterally invariant medium at the receiver level. Alternately in the $t-x$ space, the scaling can be determined by the ratio of the direct arrival's amplitude on the hydrophone and vertical geophone components at various offsets.

As emphasized above, this method assumes that all energy is pressure wave energy, and therefore everything recorded by the hydrophone should have its counterpart in the geophone data, with either positive polarity (upgoing) or negative polarity (downgoing).

Wave mode separation and imaging

The Helmholtz separation operator is based on the assumption that any isotropic vector field can be described as a combination of a scalar and vector potential fields:

$$\mathbf{u} = \nabla\Phi + \nabla \times \mathbf{\Psi}, \tag{2}$$

where Φ is the scalar potential field and $\mathbf{\Psi}$ is the vector potential. $\mathbf{u}$ is the elastic displacement vector wavefield. The scalar potential generates pressure waves, and the vector potential generates shear waves. Therefore, the Helmholtz method of separating the P-wave amplitude from the S-wave amplitude is to apply a divergence operator and a curl operator to the displacement field:

$$P = \nabla \cdot \mathbf{u} = \nabla^2\Phi; \tag{3}$$

$$\mathbf{S} = \nabla \times \mathbf{u} = -\nabla^2\Psi. \tag{4}$$

Equations 3 and 4 apply only for an isotropic medium. Dellinger and Etgen (1990) extend these operators for an anisotropic medium.

The Helmholtz separation operator is useful for distinguishing between P and S-wave amplitudes, but it is not reversible. The derivation of a reversible P-wave and S-wave displacement decomposition by Zhang and McMechan (2010) is done in the wavenumber domain. They formulate a linear equation system based on characteristics of P and S particle displacements in an isotropic elastic medium. The solutions to this linear system in a two-dimensional medium are:

$$\tilde{u}_x^P = k_x^2\tilde{u}_x + k_x k_z \tilde{u}_z, \tag{5}$$
$$\tilde{u}_z^P = k_z^2\tilde{u}_z + k_z k_x \tilde{u}_x, \tag{6}$$

and

$$\tilde{u}_x^S = k_z^2\tilde{u}_x - k_x k_z \tilde{u}_z, \tag{7}$$
$$\tilde{u}_z^S = k_x^2\tilde{u}_z - k_z k_x \tilde{u}_x, \tag{8}$$

where $\tilde{u}_i$ are the spatial fourier transforms of the observed displacement fields in direction i, k_i are the wavenumbers, and $\tilde{u}_i^P$ and $\tilde{u}_i^S$ are the decomposed P and S displacements. It is important to note that the k in these equations is normalized by the absolute value of the wavenumber $|\mathbf{k}|$. This decomposition is reversible, since $u_i = u_i^P + u_i^S$.

Forward and adjoint isotropic elastic wave propagation

The isotropic elastic wave equation relates displacements to stresses via two elastic constants - the Lam*é* parameters λ and μ:

$$\nabla\left(\left(\lambda+2\mu\right)\nabla\cdot\mathbf{u}\right)-\nabla\times\left(\mu\nabla\times\mathbf{u}\right)+\mathbf{f}=\rho\ddot{\mathbf{u}}, \tag{9}$$

where $\mathbf{u}$ are the particle displacements in each dimension, $\mathbf{f}$ is the force function and ρ is medium density. An alternate formulation is:

$$\nabla\left(\left(\lambda+\mu\right)\nabla\cdot\mathbf{u}\right)+\nabla\cdot\left(\mu\nabla\mathbf{u}\right)+\mathbf{f}=\rho\ddot{\mathbf{u}}. \tag{10}$$

From equation 10, the explicit form for a heterogeneous two dimensional medium can be expressed in a matrix-vector notation as:

$$\begin{bmatrix}\frac{1}{\rho}\partial_x\left(\left(\lambda+2\mu\right)\partial_x u_x+\lambda\partial_z u_z\right)+\frac{1}{\rho}\partial_z\left(\mu\left(\partial_x u_z+\partial_z u_x\right)\right)+\frac{1}{\rho}f_x\\ \frac{1}{\rho}\partial_z\left(\left(\lambda+2\mu\right)\partial_z u_z+\lambda\partial_x u_x\right)+\frac{1}{\rho}\partial_x\left(\mu\left(\partial_x u_z+\partial_z u_x\right)\right)+\frac{1}{\rho}f_z\end{bmatrix}=\begin{bmatrix}\partial_t^2 u_x\\ \partial_t^2 u_z\end{bmatrix}. \tag{11}$$

The forward elastic propagation operator can then be expressed as:

$$\mathbf{F}=\begin{bmatrix}\frac{1}{\rho}\partial_x\left(\lambda+2\mu\right)\partial_x+\frac{1}{\rho}\partial_z\mu\partial_z-\partial_t^2 & \frac{1}{\rho}\partial_x\lambda\partial_z+\frac{1}{\rho}\partial_z\mu\partial_x\\ \frac{1}{\rho}\partial_z\lambda\partial_x+\frac{1}{\rho}\partial_x\mu\partial_z & \frac{1}{\rho}\partial_z\left(\lambda+2\mu\right)\partial_z+\frac{1}{\rho}\partial_x\mu\partial_x-\partial_t^2\end{bmatrix} \tag{12}$$

For a homogeneous medium, and using a Green's function to describe the energy propagation between any two locations $\mathbf{x}=(x,y,z)$ and $\mathbf{y}=(x,y,z)$, the equation takes the form:

$$\left(\left(\lambda+\mu\right)\nabla\nabla+\mu\nabla^2+\rho\omega^2\right)G\left(\mathbf{x},\mathbf{y},\omega\right)=-\delta\left(\mathbf{x}-\mathbf{y}\right) \tag{13}$$

The forward elastic propagation operator injects sources from a model into some location in the medium, and records the resulting wavefield at some other location:

$$d\left(\mathbf{x},\omega;\mathbf{x}_s\right)=\sum_{\mathbf{y}}m\left(\mathbf{y},\omega;\mathbf{x}_s\right)G\left(\mathbf{y},\mathbf{x},\omega\right), \tag{14}$$

where m is the model of injected sources at location $\mathbf{y}$ in the medium, and d are the recorded displacement fields $\mathbf{u}$ at location $\mathbf{x}$ in the medium. ω is angular frequency and $\mathbf{x}_s$ is the shot gather. In vector notation, this is expressed as

$$\mathbf{d}=\mathbf{F}\mathbf{m}, \tag{15}$$

where $\mathbf{F}$ is the forward operator. The adjoint operator injects the data from the same recording locations, and records the resulting wavefield at the model injection points:

$$\tilde{m}\left(\mathbf{y},\omega;\mathbf{x}_s\right)=\sum_{\mathbf{x}} d\left(\mathbf{x},\omega;\mathbf{x}_s\right) G^*\left(\mathbf{x},\mathbf{y},\omega\right), \tag{16}$$

which in vector notation is

$$\tilde{\mathbf{m}}=\mathbf{F}^*\mathbf{d}, \tag{17}$$

where $\mathbf{F}^*$ is the adjoint operator.

Inverting for the virtual source model

The inversion is done by least-square fitting of modeled geophone data to the recorded geophone data. The model is a virtual-source array, injected into some locations in a homogeneous medium. There should be some distance between these virtual-sources' locations and the receiver line where the displacement fields will be recorded. This distance is necessary for the recreated wavefield to form.

It is not possible to recreate the entire original wavefield that was recorded by the geophones without accurate knowledge of the acquisition geometry and the medium parameters. However, given a particular acquisition geometry, and some reasonable medium parameters, it is possible to recreate the original wavefield in the vicinity of the geophones. This wavefield will form as a result of the injection of the virtual sources, and will become more similar to the originally recorded wavefield at the receiver locations as it propagates toward them.

The inversion starts from a zero-value initial model of displacement sources $\mathbf{m}^0=\mathbf{0}$. This initial model is injected as a displacement force function, at locations $\mathbf{x}$ in the medium. The energy is propagated with the forward elastic operator, and recorded at locations $\mathbf{y}$ in the medium (the receiver locations):

$$\mathbf{d}=\mathbf{F}\mathbf{m}^{\mathbf{0}}. \tag{18}$$

The residual that must be minimized is the difference between the calculated data d, and the observed data d_{obs}. The objective function is:

$$J(\mathbf{m})=\|\mathbf{d}-\mathbf{d}_{\text{obs}}\|_2^2=\|\mathbf{F}\mathbf{m}-\mathbf{d}_{\text{obs}}\|_2^2. \tag{19}$$

The model gradient is:

$$\mathbf{\Delta m}=\frac{\partial J}{\partial \mathbf{m}}=\left(\frac{\partial \mathbf{r}}{\partial \mathbf{m}}\right)^T\mathbf{r}=\mathbf{F}^*\mathbf{r}, \tag{20}$$

where $\mathbf{F}^*$ is the adjoint elastic propagation operator. The data gradient is the forward operator applied to the model gradient:

$$\mathbf{\Delta r} = \mathbf{F}\mathbf{\Delta m}. \tag{21}$$

The model gradient and the data residual are updated using an itterative minimization scheme (Claerbout and Fomel, 2011).

The end result of the inversion is the model $\mathbf{m}$ which, when injected at locations $\mathbf{x}$ in a homogeneous medium with the parameters used in the inversion, will generate recorded data at locations $\mathbf{y}$ that are equal to the observed data. Even if the medium parameters that were used to generate the wavefield were not a good approximation to the true parameters, this difference will be minor with regard to the wavefield at a close proximity to the receivers. Therefore, if the data residual is zero, we can assume that the wavefield near the receivers has likewise been reliably recreated.

The displacement field values are calculated for all time steps by running the forward propagation operator using the final virtual-source model as an input:

$$F \begin{bmatrix} -\frac{1}{\rho} m_x \\ -\frac{1}{\rho} m_z \end{bmatrix} = \begin{bmatrix} u_x \\ u_z \end{bmatrix}. \tag{22}$$

The separation operators in equations 3 and 4 are applied to the displacements fields (u_x, u_z) at the receiver locations, in order to separate P-wave amplitudes from S-wave amplitudes. These operators require calculating spatial derivatives of the displacement fields in the horizontal and vertical directions. We now have omnidirectional wavefield values near the receivers, therefore applying these operators to the recreated wavefields will result in an approximation to the actual P and S-waves that were recorded by the geophones. Furthermore, the displacement separation operators in equations 6-8 can be used to separate P displacements from S displacements.

INVERSION RESULTS

Synthetic land data 1

The first set of examples are of synthetic land data. The data are a single shot gather, forward modeled using an elastic isotropic migration code which utilizes the stress-displacement formulation, and a staggered-grid finite-difference scheme (Virieux, 1986). The medium parameters are shown in Figure 2. The source was a pressure source, located on the surface at the center of the model. A free boundary condition was used for the upper boundary, and absorbing boundaries were used for the bottom and the sides. The receivers were split-spread around the source, up to a maximum offset of $1800m$. The direct arrival has been muted from the synthetic data.

The recorded vertical and horizontal displacements are shown in Figures 3(a)-3(b). These represent the geophone data. The P-wave and S-wave shown in Figures 3(c)-3(d) are calculated from the displacement field with the Helmholtz separation operator in equations 3-4.

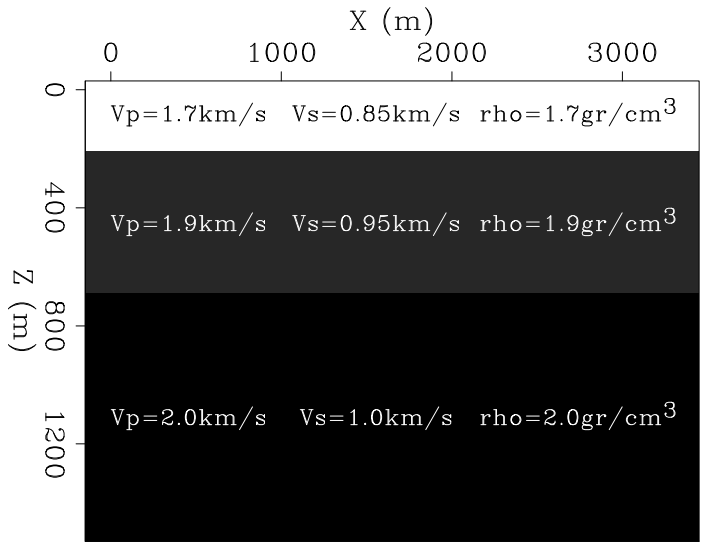

Figure 2: Medium parameters of synthetic land data. [**ER**]

Figure 4 shows the arrangement of the virtual sources and the receivers during the inversion. The virtual-source line is longer than the receiver line to better facilitate the modeling of high-wavenumber waves, which may be present at the edges of the recorded data. The medium itself is homogeneous, and surrounded by absorbing boundaries. The elastic propagation finite-difference scheme used in the inversion is different from the one used for generating the synthetic data. It utilizes a displacement-only formulation (as in equation 11), on a regular grid. The finite-difference approximation is 2_{nd} order in time and in space.

The vertical and horizontal virtual-source models resulting from the inversion are shown in Figures 5(a) and 5(b). When these source functions are injected as displacement sources into the homogeneous medium which was used in the inversion, the results are the reconstructed displacement data. If the inversion converged, then these reconstructed data will be equal to the recorded geophone data. The purpose of Figures 6(a)-6(h) is to show that the inversion managed to converge, even when the medium parameters used were different from the true ones.

The P-wave velocity at the receiver level in the medium used for forward modeling was $1700\frac{m}{s}$, S-wave velocity was $850\frac{m}{s}$ and density was $1.7\frac{gr}{cm^3}$. Figures 6(a) and 6(b) are the forward modeled displacements. Figures 6(c) and 6(d) are the reconstructed displacements when using the correct medium parameters in the inversion. Figures 6(e) and 6(f) are the reconstructed displacements when using a homogeneous medium with $V_p = 1500\frac{m}{s}$, $V_s = 700\frac{m}{s}$ and $\rho = 1.5\frac{gr}{cm^3}$ (i.e. - about 15% too slow). Figures 6(g) and 6(h) are the reconstructed displacements when using a homogeneous medium with $V_p = 2000\frac{m}{s}$, $V_s = 1000\frac{m}{s}$ and $\rho = 2.0\frac{gr}{cm^3}$ (i.e. - about 15% too fast). Note that the displacements at the receivers have indeed been matched.

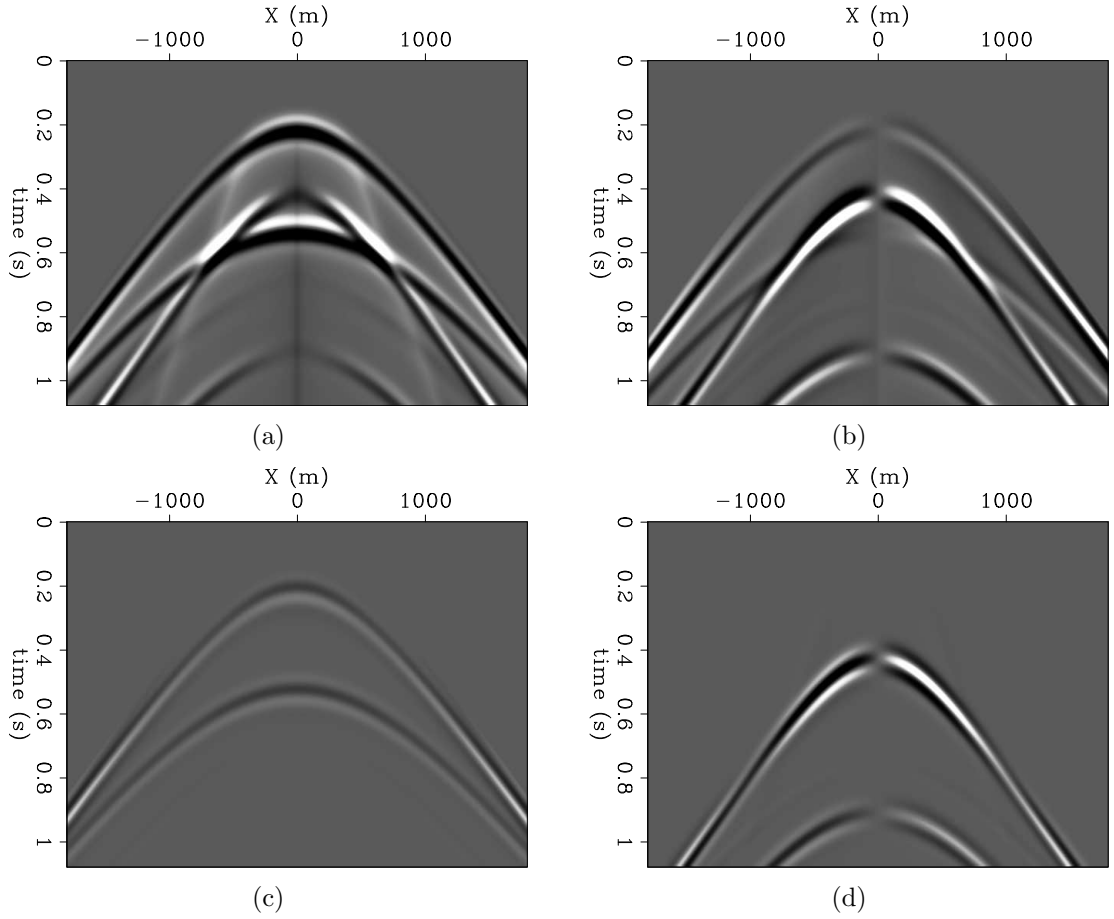

Figure 3: Synthetic land data. (a) vertical displacement, (b) horizontal displacement, (c) P-wave, (d) S-wave. [**ER**]

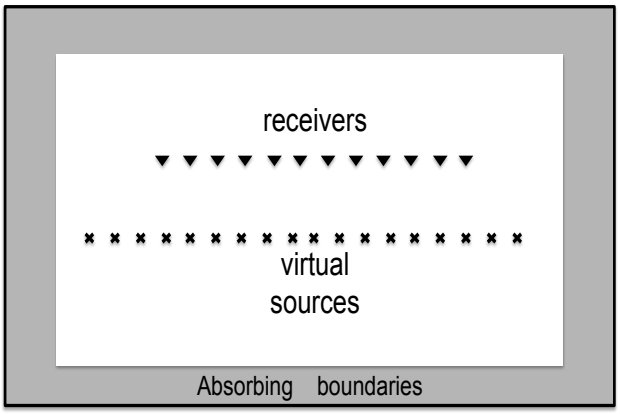

Figure 4: Qualitative sketch depicting the relative locations of the receivers and the virtual sources used in the inversion. The virtual source line has a greater horizontal extent than the receivers in order to enable convergence to a solution when high wavenumbers exist at the sides of the recorded data. [**NR**]

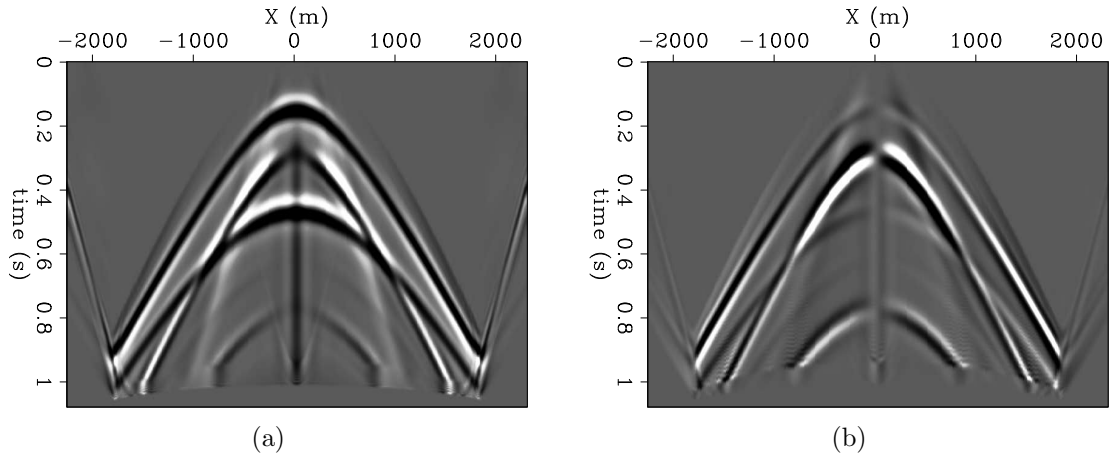

Figure 5: The virtual source functions that generate the observed land data. These "models" are the inversion results. (a) vertical displacement source functions, (b) horizontal displacement source functions. [**ER**]

Figures 7(a)-8(d) are the result of applying the Helmholtz separation operator to the reconstructed displacement fields, to calculate the P and S-waves. The finite-difference approximation to the Helmholtz operator uses the displacement value at the receivers (which have been matched), and also the values one depth level below the receivers. These values are not matched by the inversion, and therefore unless the medium parameters are correct - they will not be an accurate representation of the true field values there. This will cause the vertical derivative to be inaccurate as well. The question then is: how detrimental are such inaccuracies to the P/S separation result?

Figure 7(a) is the forward modeled and separated synthetic P-wave recording. Figure 7(b) is the reconstructed P recording, when using the correct medium parameters in the inversion. Figure 7(c) is the reconstructed P when using a 15% too slow homogeneous medium, and Figure 7(d) is for a 15% too fast homogeneous medium. Figure 7(e) is a summation of the forward modeled and separated P and S recording, and is useful for estimating the separation quality for each scenario.

In Figure 7(b), the reconstructed P-wave is almost identical to the forward modeled P-wave, while the S-wave is barely visible. This indicates that the reconstructed displacement fields were a good approximation of the forward modeled displacement fields. In Figures 7(c) and 7(d) the medium parameters are incorrect, and the S-wave is more visible. However, the separation quality is still reasonable, when compared to Figure 7(e). This indicates that though the medium parameters were off by 15%, the displacement fields were a good approximation to the forward modeled fields one depth step below the receivers (as well as at the receivers themselves). Therefore, the vertical derivatives of the displacement fields reasonably approximate the true derivatives, and the P separation (equation 3) is effective.

Figure 8(a) is the synthetic S-wave recording. Figure 8(b) is the reconstructed S

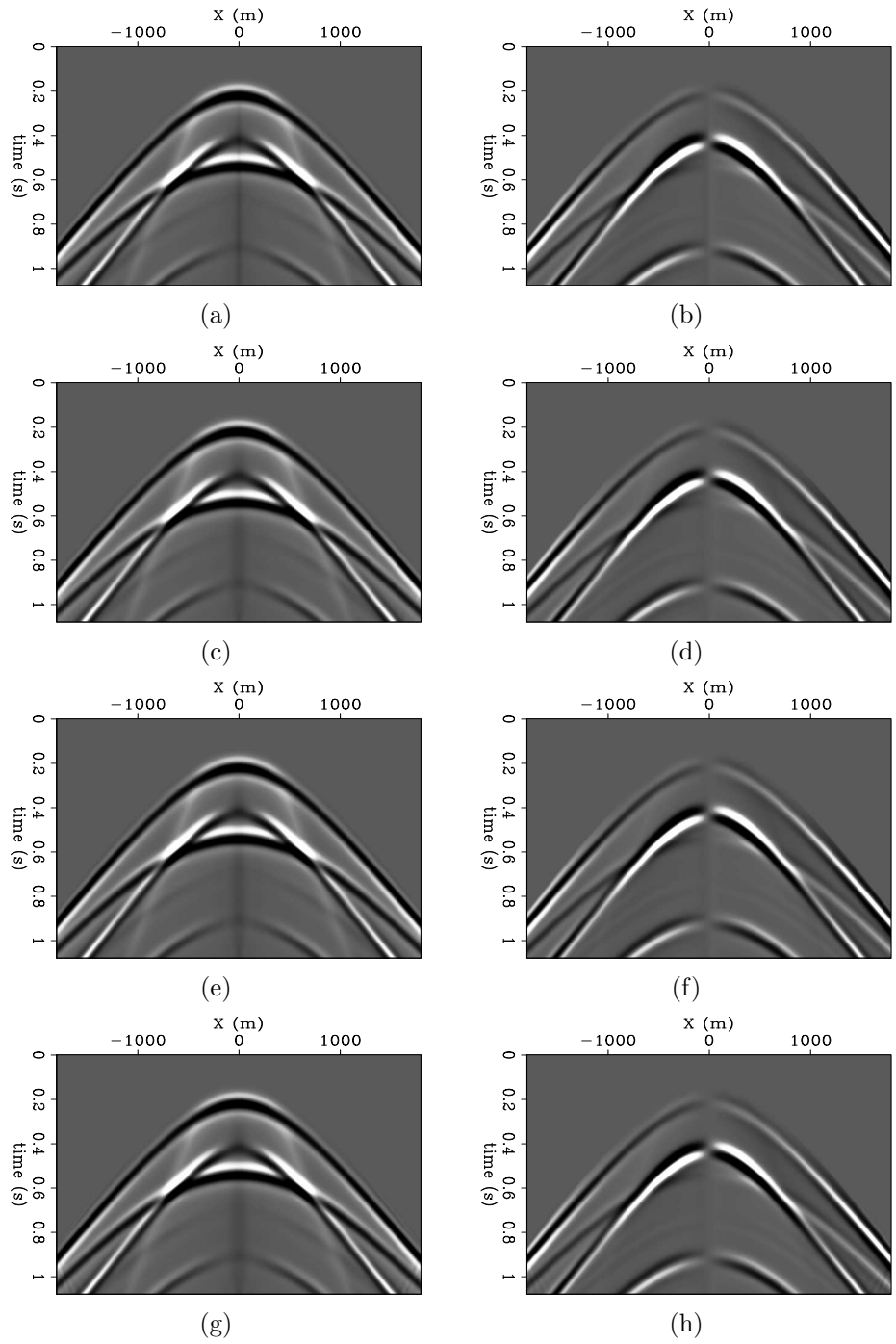

Figure 6: Synthetic and reconstructed displacements of land data. (a) synthetic vertical displacement, (b) synthetic horizontal displacement, (c) reconstructed vertical displacement with correct velocity, (d) reconstructed horizontal displacement with correct velocity, (e) reconstructed vertical displacement with 15% too slow velocity, (f) reconstructed horizontal displacement with 15% too slow velocity, (g) reconstructed vertical displacement with 15% too fast velocity, (h) reconstructed horizontal displacement with 15% too fast velocity. [**ER**]

recording, when using the correct medium parameters in the inversion. Figure 8(c) is the reconstructed S when using a 15% too slow homogeneous medium, and Figure 8(d) is for a 15% too fast homogeneous medium. Figure 8(e) is the sum of the forward modeled P and S. As for the previous set of figures, we can see that the separation quality does decrease as the medium parameters vary from the true ones, but the separation is still of reasonable quality even when the parameters are off by a large percentage.

There is an additional effect of the inversion modeling process, which is visible in this set of figures and particularly in Figure 8(b). As a result of the edges of the receiver line, a diffraction is generated at both ends during the adjoint propagation, and this diffraction is recorded at the virtual-source line. It can be seen in the virtual-source functions, in Figures 5(a)-5(b). The recording of this diffraction event is then repropagated during the forward propagation stage of the inversion, generating an additional diffraction event off the edges of the virtual-source line. This diffraction event was not part of the original wavefield. Since it arrives at the same time as the first P-wave, it is not visible in Figures 7(b)-7(d), but it is visible in Figures 8(b)-8(d), even when using the correct velocity for the inversion.

Synthetic land data 2

The next set of examples are also of synthetic land data, but they represent a scenario where the velocity at the recording surface varies laterally. Three shot gathers were generated in three separate homogeneous mediums, with differing medium parameters. For each gather there was a different random reflection series. The gathers were then summed to simulate a variable surface velocity.

The forward modeling medium parameters were:

1. Gather 1: $v_{p1} = 2000\frac{\text{m}}{\text{s}}$, $v_{s1} = 1000\frac{\text{m}}{\text{s}}$, $\rho_1 = 2.0\frac{gr}{cm^3}$
2. Gather 2: $v_{p2} = 1800\frac{\text{m}}{\text{s}}$, $v_{s2} = 900\frac{\text{m}}{\text{s}}$, $\rho_2 = 1.8\frac{gr}{cm^3}$
3. Gather 3: $v_{p3} = 1600\frac{\text{m}}{\text{s}}$, $v_{s3} = 800\frac{\text{m}}{\text{s}}$, $\rho_3 = 1.6\frac{gr}{cm^3}$

Figures 9(a) and 9(b) are the vertical and horizontal displacements. Figures 9(c) and 9(d) are the P and S-waves calculated by applying the Helmholtz separation operators. Three different reflection groups can be discerned in the synthetic data. The left group corresponds to the fastest medium, the central group to the intermediate medium, and the right group to the slowest medium.

There were three inversion runs, each one with different homogeneous medium parameter sets:

1. Inversion 1 (intermediate): $v_{p1} = 1700\frac{\text{m}}{\text{s}}$, $v_{s1} = 850\frac{\text{m}}{\text{s}}$, $\rho_1 = 1.7\frac{gr}{cm^3}$

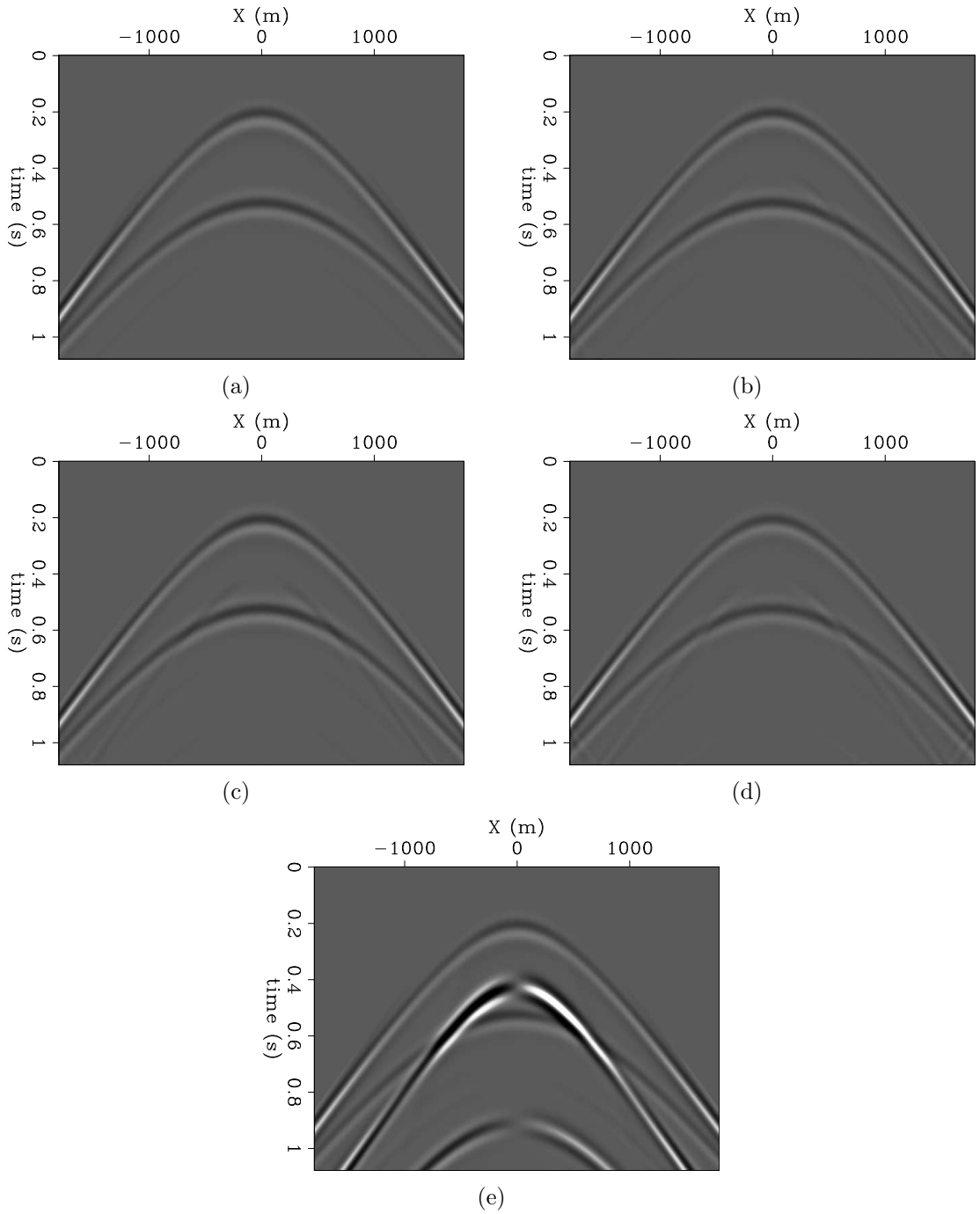

Figure 7: Synthetic and reconstructed P-wave of land data. (a) Synthetic P, (b) reconstructed P with correct velocity, (c) reconstructed P with 15% too slow velocity, (d) reconstructed P with 15% too fast velocity, (e) sum of synthetic P and S-waves. All figures are identically clipped. [**ER**]

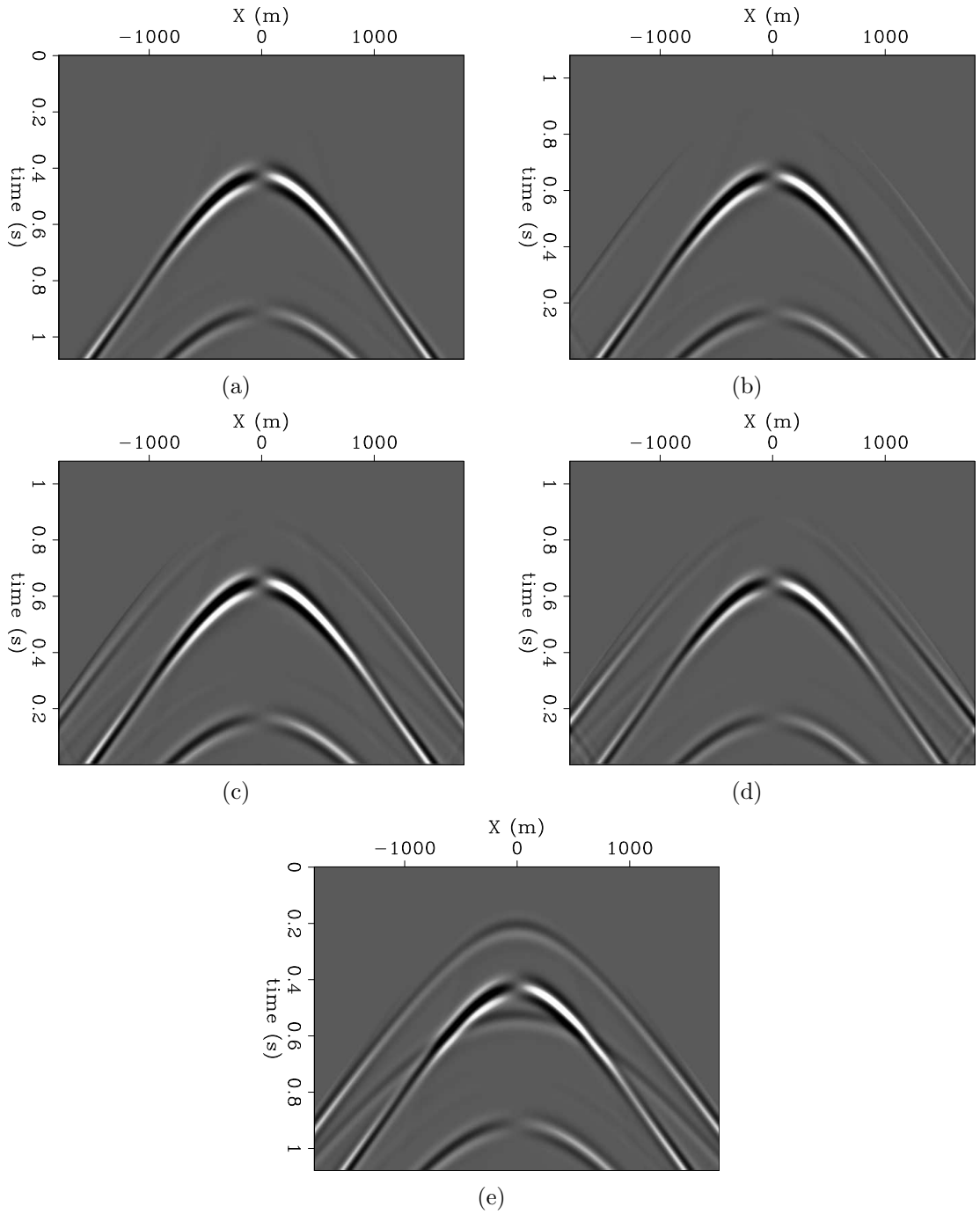

Figure 8: Synthetic and reconstructed S-wave of land data. (a) Synthetic S, (b) reconstructed S with correct velocity, (c) reconstructed S with 15% too slow velocity, (d) reconstructed S with 15% too fast velocity, (e) sum of synthetic P and S-waves. All figures are identically clipped. [**ER**]

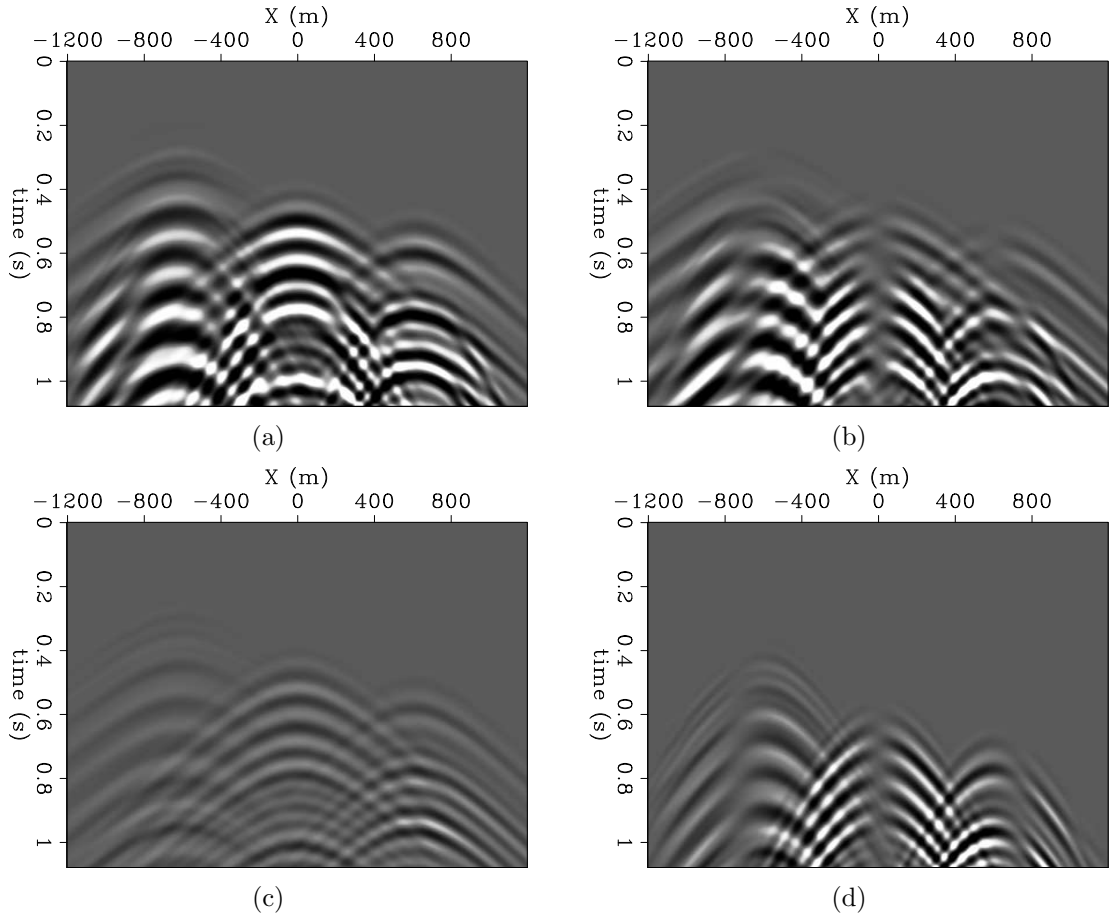

Figure 9: Synthetic land data. (a) vertical displacement, (b) horizontal displacement, (c) P-wave, (d) S-wave. [**ER**]

2. Inversion 2 (slow): $v_{p2} = 1500\frac{\text{m}}{\text{s}}$, $v_{s2} = 700\frac{\text{m}}{\text{s}}$, $\rho_2 = 1.5\frac{gr}{cm^3}$
3. Inversion 3 (fast): $v_{p3} = 2000\frac{\text{m}}{\text{s}}$, $v_{s3} = 1000\frac{\text{m}}{\text{s}}$, $\rho_3 = 2.0\frac{gr}{cm^3}$

The medium parameters of inversion 3 match those of the fast events, but are different from the parameters used to generate the intermediate and the slow events. As for the medium parameters of inversions 1 and 2, they match none of the parameters used to generate the datasets. For inversion 2, the velocity error is up to 33% (compared to the fast arrivals). The inversions were run until a good match to the displacement data was achieved.

Figures 10(a)-10(e) show the reconstructed P-waves. Figure 10(a) is the synthetic P recording. Figure 10(b) is the P reconstruction calculated from the displacements of the inversion with parameter set 1 (intermediate). Figure 10(c) is the P reconstruction from the inversion using parameter set 2 (slow), and Figure 10(d) is from parameter set 3 (fast). Figure 10(e) is the summation of the synthetic P and S recordings, and is a visual aid to estimate the separation quality for each scenario.

Since the intermediate parameter set 1 has the least error in comparison to the media with which the forward modeled data were generated, the reconstructed P-wave is most accurate for it, as seen in Figure 10(b). However, the other two P-wave reconstructions show reasonable separation quality, despite the large error in medium parameters. The same can be said for the next set of S-wave separation results in Figures 11(a)-11(e). The best separation is where the medium parameter error is minimal (Figure 11(b)). However, even where the error is large (Figures 11(c) and 11(d)), the separation results, though not being great, are still reasonably good compared to the synthetic data.

Synthetic OBS data

The next result set is of OBS data, and its purpose is to show the problem that the inversion method described above has when both upgoing and downgoing data are present. For that same purpose, the synthetic data were forward modeled without shear waves (i.e. - $V_s = 0$).

The medium parameters used for forward modeling are shown in Figure 12. The top layer is water. Shear velocity was set to zero everywhere. The source was a pressure source, located on the water surface, at the center of the model. The receivers were located at the top of the second layer, which represents sediment. The upper boundary was free, and the sides and bottom of the model had absorbing boundaries. The direct arrival was muted.

The inversion was run using the correct P-wave velocity and density (those of the sediment in which the receivers were placed), but also with shear-wave velocity set to $850\frac{m}{s}$. The virtual-sources were placed below the receivers, as shown in Figure 4.

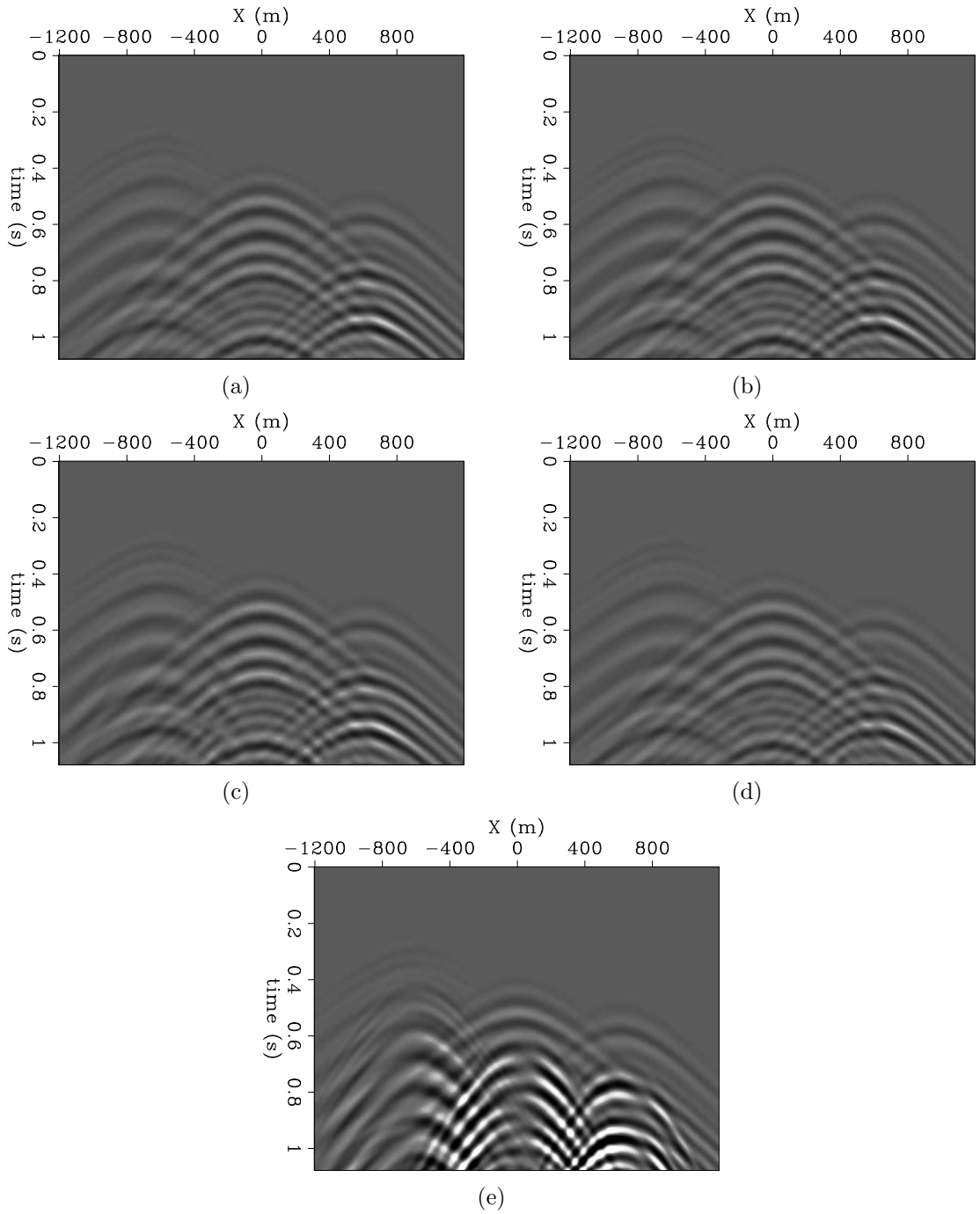

Figure 10: Synthetic and reconstructed P-wave of land data. (a) Synthetic P, (b) reconstructed P with intermediate medium parameters, (c) reconstructed P with slow parameters, (d) reconstructed P with fast parameters, (e) sum of synthetic P and S-waves. All figures are identically clipped. [**ER**]

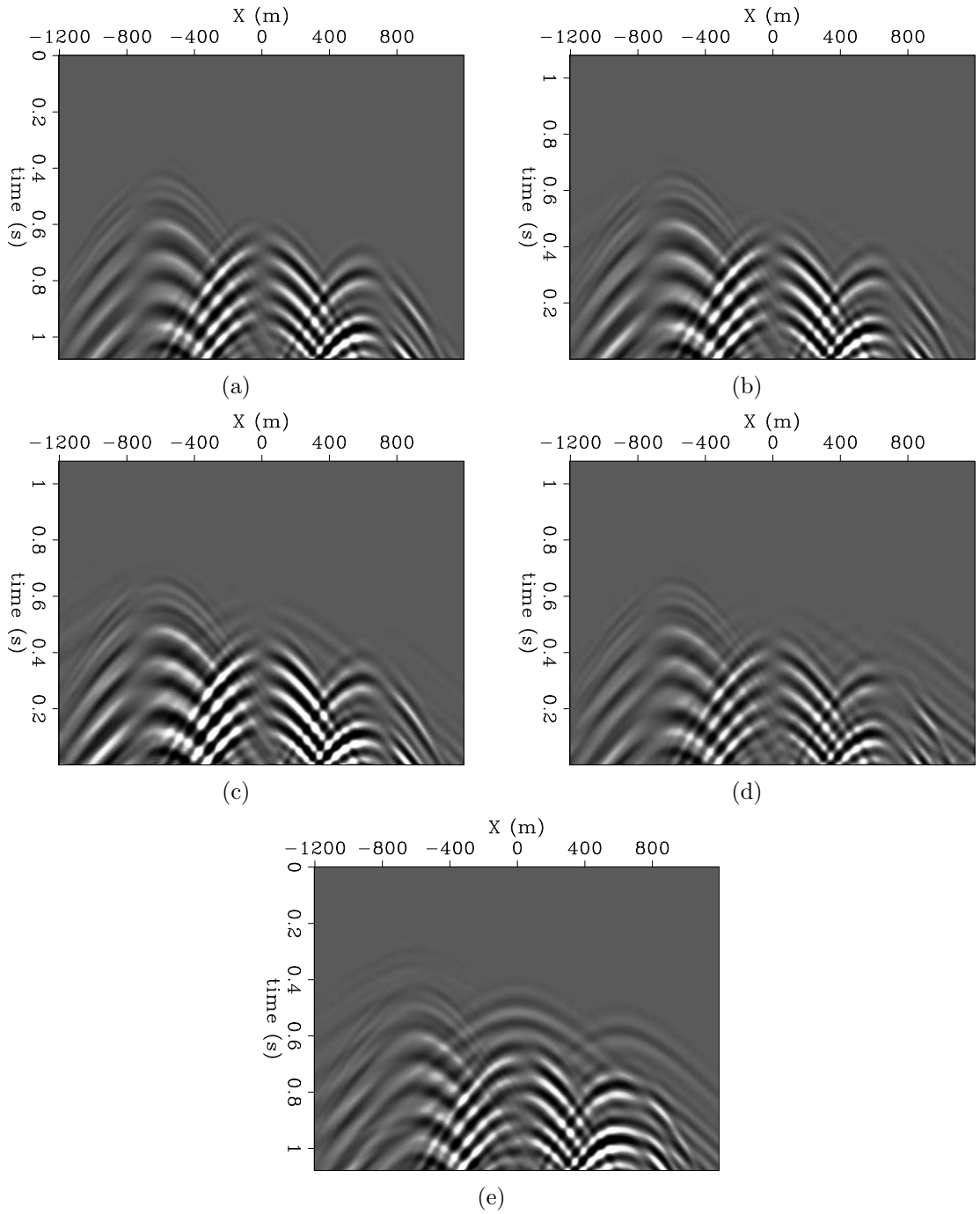

Figure 11: Synthetic and reconstructed S-wave of land data. (a) Synthetic S, (b) reconstructed S with intermediate medium parameters, (c) reconstructed S with slow parameters, (d) reconstructed S with fast parameters, (e) sum of synthetic P and S-waves. All figures are identically clipped. [**ER**]

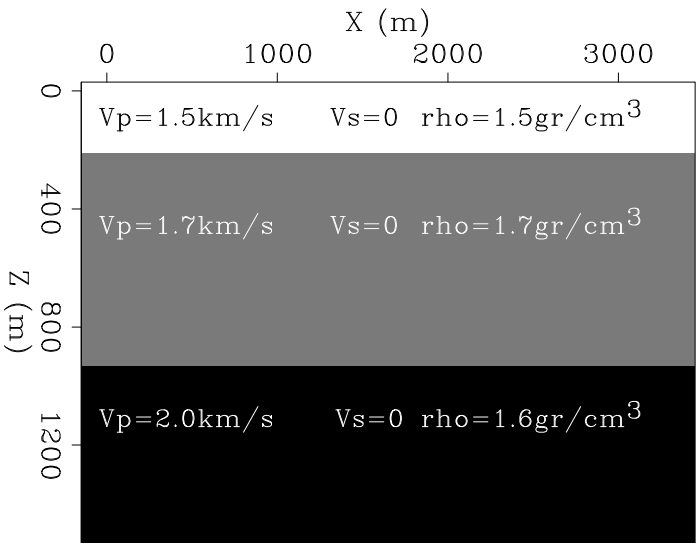

Figure 12: Medium parameters of synthetic OBS data. Shear velocity was zero everywhere. [**ER**]

The synthetic vertical and horizontal displacement data are shown in Figures 13(a) and 13(b). Of the five events visible, the first, second, fourth and fifth arrivals are downgoing waves, reflected off the water surface. The only upgoing wave is the third arrival.

The reconstructed displacements are in Figures 13(c) and 13(d). These figures show that the objective function has indeed been minimized, and the displacement data have been matched.

Figure 14(a) shows the P-wave recording, obtained by the Helmholtz separation operator applied to the synthetic displacement fields. Figure 14(b) is a validation that there are no S-waves present in the synthetic data. Figure 14(c) is the reconstructed P-waves calculated by the Helmholtz P-wave separation operator applied to the reconstructed displacements. Note that all the downgoing events have an opposite polarity compared to the synthetic P section, while the only P event that was reconstructed with the correct polarity is the upgoing arrival (the third arrival). The amplitude of the reconstructed third arrival is stronger than its amplitude in the synthetic P section.

Figure 14(d) is the Helmholtz S-wave separation operator applied to the reconstructed displacements. It shows that for every P arrival, a shear arrival was reconstructed as well, despite the fact that there were no shear waves in the synthetic wavefield.

The reason for the inaccuracy of the P and S-wave reconstruction in this case is that as a result of the virtual-sources being below the receivers, only upgoing waves could be modeled by the inversion. The inversion does generate a match to the displacement data, but the displacements are unconstrained above and below the receivers. Therefore the inversion is free to explain the downgoing P-waves as a combination of (incorrect) upgoing P-waves and upgoing S-waves. A graphical explanation of this feature is shown in Figure 15. The grey area represents the possible

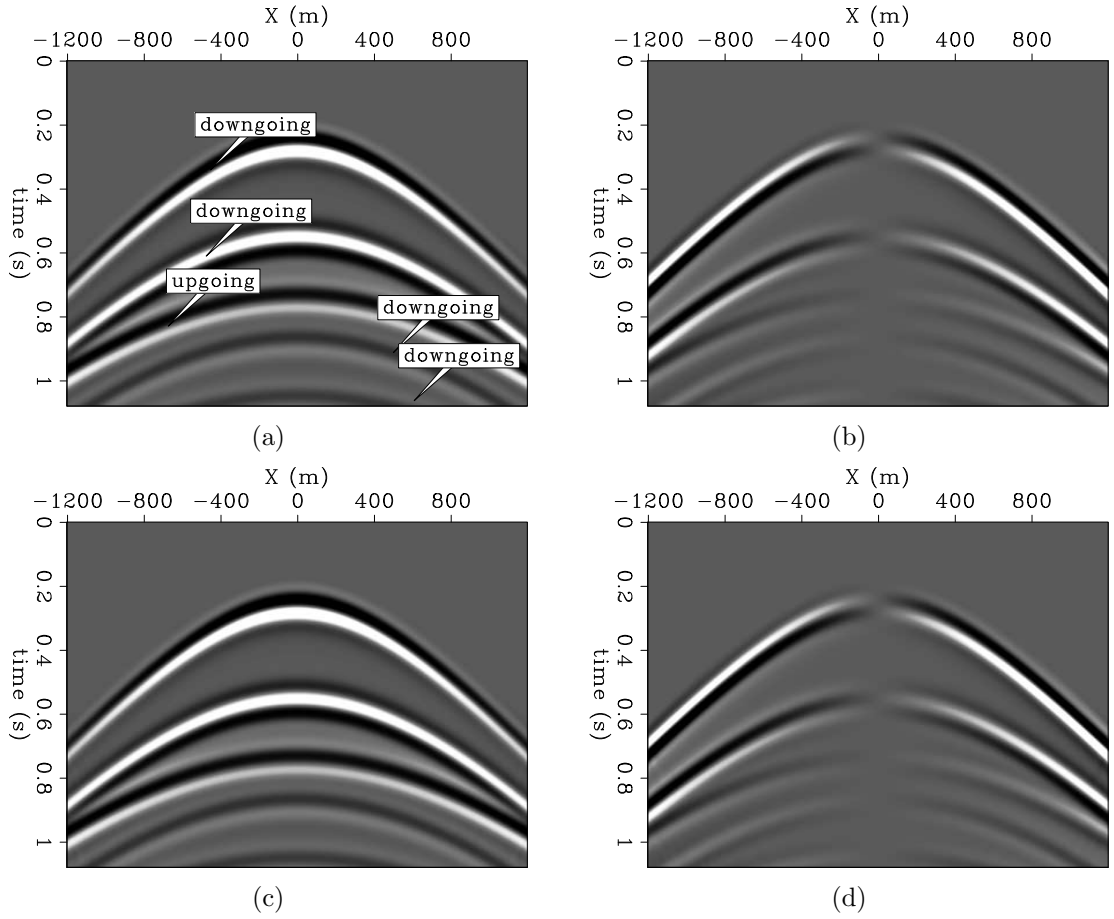

Figure 13: Synthetic and reconstructed OBS data. (a) synthetic vertical displacement, (b) synthetic horizontal displacement, (c) reconstructed vertical displacement, (d) reconstructed horizontal displacement. [**ER**]

downgoing wave solutions which were not enabled by this inversion configuration. Instead, the incorrect upgoing wave modes (which still match the displacement data at the receivers and are therefore a possible solution) are used to explain the downgoing energy.

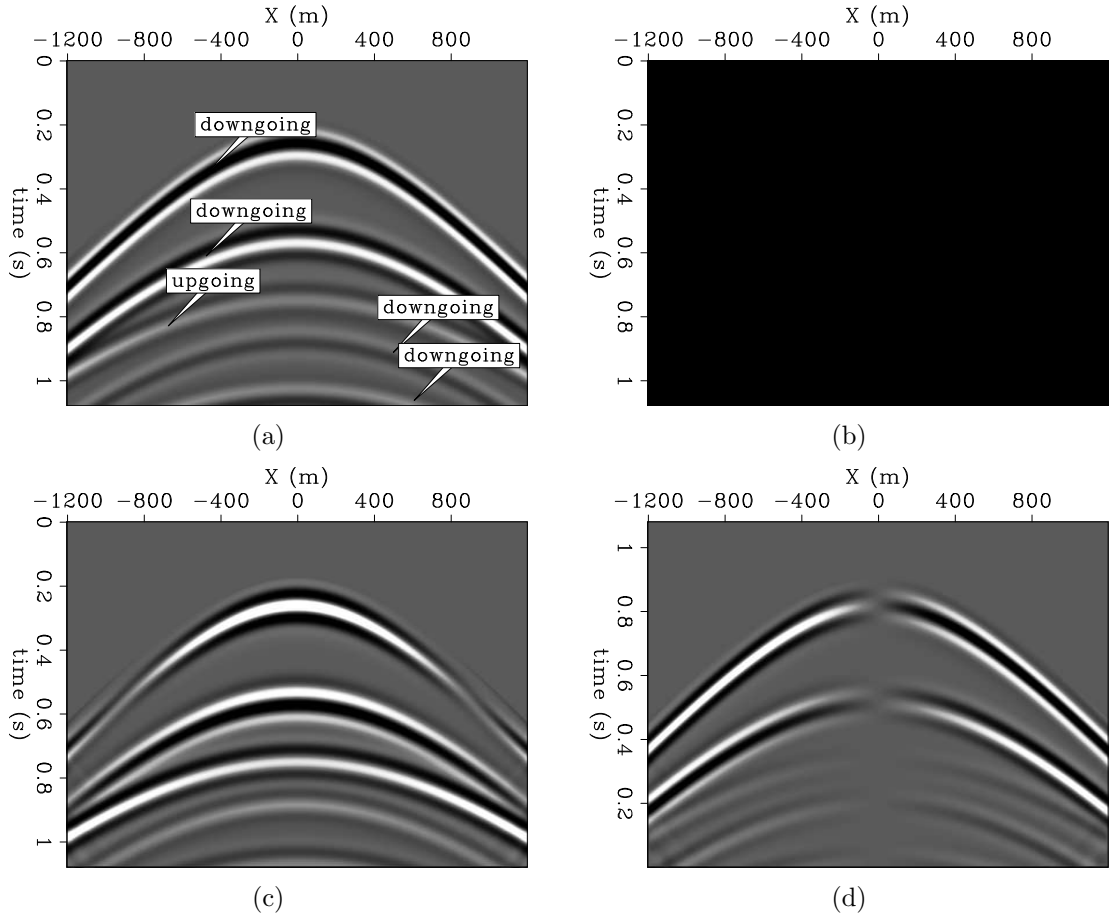

Figure 14: Synthetic and reconstructed OBS data. (a) synthetic P-wave, (b) synthetic S-wave, (c) reconstructed P-wave, (d) reconstructed S-wave. [**ER**]

DISCUSSION AND CONCLUSION

The more the homogeneous medium parameters used in the inversion differ from the true medium parameters in which the receivers were placed, the less accurate is the reconstructed wavefield in the proximity of the receivers. This in turn means that the spatial derivatives will differ from the true derivatives, and thus the separation of P-waves from S-waves will be less reliable. However, given the typical length of seismic waves in exploration geophysics, and the spatial oversampling used in finite-difference modeling, the inaccuracy in medium parameters for which this separation method can still function reliably is quite large.

The locations of virtual sources in relation to the receivers determine what wavenum-

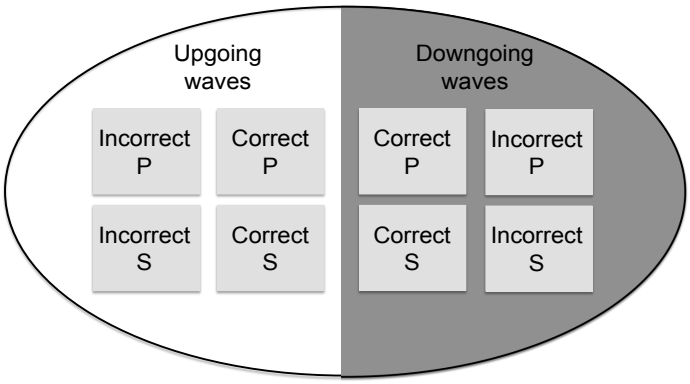

Figure 15: Representation of the solution space of the inversion. If the data contain both upgoing and downgoing waves, but the inversion is unable to reconstruct the downgoing waves, then incorrect P and S-waves will be used to match the observed geophone data. [**NR**]

bers can be reconstructed. In order to accurately recreate all wavenumbers in the data, the virtual-sources must be placed in a configuration that enables the generation of those wavenumbers. For land data, the implication is that virtual-sources should be placed below the receivers. For OBS data, this should mean that virtual-sources must be placed above and below the receivers. However, such a configuration drastically increases the null-space of the inversion, and the results (not shown here) are very noisy and inaccurately reconstructed P and S sections.

I am currently investigating two possible avenues for implementing the inversion successfully on OBS data. The first possibility is to run the inversion twice: once with virtual-sources below the receivers, and once with virtual-sources above. The shear waves propagate upward only, and will be reconstructed by the upgoing inversion. As can be seen from Figures 14(a) and 14(d), the downgoing P-waves are reconstructed with opposite polarity when the virtual-sources are below the receivers. Likewise, the upgoing P-waves will be reconstructed with an opposite polarity when the virtual-sources are above the receivers. By comparing the polarity reversals to the observed hydrophone data, it is possible to gauge which P events are improperly reconstructed. I am searching for a way to introduce the hydrophone data as a constraint to the objective function, so that the polarity reversal attribute can be used to guide the inversion.

The second possibility is to have the virtual-sources below the receivers, but use a reflecting upper boundary, thereby recreating the downgoing waves generated by reflections off the sea surface. This configuration is not trivial to implement, since there is an important condition that has to be met: The free surface should not generate a mode conversion. If it does, downgoing shear waves will be present in the reconstructed displacement fields, and such waves definitely do not exist in OBS data.

One way of preventing a mode conversion from the free upper boundary is to use a medium with no shear strength. The possible configuration then is a line of receivers placed in a medium with parameters approximating those of the sea bottom. Above these receivers the medium will be water. Effectively, a homogeneous elastic medium underlying a homogeneous acoustic medium. The added value such a configuration may give is not only in the enabling of reconstruction of downgoing P-waves, but also

in the possibility of reconstructing the surface waves.

ACKNOWLEDGMENTS

I wish to thank my colleagues, Mandy, Elita, Ali, and Sjoerd for the hours (weeks, actually) of fruitful discussions, and my advisors, Prof. Ronen and Prof. Biondi, for their helpful suggestions and patience.

REFERENCES

Amundsen, L., 1993, Wavenumber-based filtering of marine point-source data: Geophysics, **58**, 1497–150.

Barr, F. J. and J. I. Sanders, 1989, Attenuation of water-column reverberations using pressure and velocity detectors in a water-bottom cable: SEG expanded abstracts, **8**, 653–656.

Claerbout, J. F. and S. Fomel, 2011, Image estimation by example: Geophysical soundings image construction.

Dankbaar, J. W. M., 1985, Separation of P- and S-waves: Geophysical Prospecting, **33**, 970–986.

Dash, R., G. Spence, R. Hyndman, S. Grion, Y. Wang, and S. Ronen, 2009, Wide-area imaging from OBS multiples: Geophysics, **74**, Q41–Q47.

Dellinger, J. and J. Etgen, 1990, Wave-field separation in two-dimensional anisotropic media: Geophysics, **55**, 914–919.

Paffenholz, J., P. Docherty, R. Shurtleff, and D. Hays, 2006, Shear wave noise on OBS Vz data - part ii: Elastic modeling of scatterers in the seabed: EAGE extended abstracts, 68th conference and exhibition, **A072**.

Robertsson, J. O. A. and E. Muyzert, 1999, Wavefield separation using a volume distribution of three component recordings: Geophys.. Res. Lett., **26**, 2821–2824.

Schalkwijk, K. M., C. P. A. Wapenaar, and D. J. Verschuur, 2003, Adaptive decomposition of multicomponent ocean-bottom seismic data into downgoing and upgoing p- and s-waves: Geophysics, **68**, 1091–1102.

Virieux, J., 1986, P-sv wave propagation in heterogeneous media: Velocity-stress finite difference method: Geophysics, **51**, 889–901.

Wapenaar, C. P. A., P. Herrmann, D. J. Verschuur, and A. J. Berkhout, 1990, Decomposition of multicomponent seismic data into primary P- and S-wave responses: Geophysical Prospecting, **38**, 663–661.

Zhang, Q. and G. McMechan, 2010, 2d and 3d elastic wavefield vector decomposition in the wavenumber domain for vti media: Geophysics, **75**, D13–D26.

Zhou, Y., C. Kumar, and I. Ahmed, 2011, Ocean bottom seismic noise attenuation using local attribute matching filter: SEG Expanded Abstracts, 81st Annual Meeting, 3586–3590.